Independent control of the shape and composition of ionic nanocrystals through sequential cation exchange reactions

Joseph M. Luther, Haimei Zheng, Bryce Sadtler, A. Paul Alivisatos
Materials Science Division, Lawrence Berkeley National Laboratory and Department of Chemistry, University of California, Berkeley

Size- and shape-controlled nanocrystal growth is intensely researched for applications including electro-optic, catalytic, and medical devices. Chemical transformations such as cation exchange overcome the limitation of traditional colloidal synthesis, where the nanocrystal shape often reflects the inherent symmetry of the underlying lattice. Here we show that nanocrystals, with established synthetic protocols for high monodispersity, can be templates for independent composition control. Specifically, controlled interconversion between wurtzite CdS, chalcocite Cu_2S, and rock salt PbS occurs while preserving the anisotropic dimensions unique to the as-synthesized materials. Sequential exchange reactions between the three sulfide compositions are driven by the disparate solubilites of the metal ion exchange pair in specific coordinating molecules. Starting with CdS, highly anisotropic PbS nanorods are created, which serve as an important material for studying strong 2-dimensional quantum confinement, as well as for optoelectronic applications. Furthermore, interesting nanoheterostructures of CdS|PbS are obtained by precise control over ion insertion and removal.

Rational design of nanoparticles has led to material systems with fascinating properties.[1-5] The combination of composition and morphology programs specific functionality in nanocrystals (NCs) for incorporation into novel device architectures. For example, anisotropic nanorods and nanotetrapods, are used in photovoltaic devices, where 2-dimensional quantum confinement controls the semiconductor bandgap and the elongated third dimension improves electron transport compared with spherical nanocrystals in bulk heterojunction devices.[6] CdSe nanorods show shape-dependent polarized photoluminescence.[7] Noble metal particles with shape control give rise to differing plasmonic activity, thus allowing for multicolor cellular labeling.[8,9] Metal nanoparticles shapes with more edge atoms also show enhanced catalysis properties. Fundamental studies of electrical transport in single nanocrystals become feasible through the controlled growth of 1D nanostructures, where different sites along the nanostructure can be independently contacted.[10-12] Therefore, in addition to size and composition, the shape control of nanocrystals demonstrates an important variable to adapt the properties for various applications.

Solution-phase synthetic methods for colloidal nanocrystals are intensely studied as we envision and design specific shapes for combinations of properties.[13-16] However, in the traditional nucleation and growth, their resulting size, shape and composition are often interdependent. Methods for independently tuning one parameter (e.g. composition), while preserving the other two (e.g. size and shape) would enable more systematic control over the resulting nanocrystal properties. We and others have demonstrated that ionic nanocrystals can be used as starting materials where the composition is altered post synthesis by exchanging either the cation or anion with

a substitutional ion from solution.[17-19] For example, CdSe nanocrystals can be converted to Ag_2Se with surprising efficiency by simply injecting an alcoholic solution of Ag^+ ions into a suspension of CdSe nanocrystals in toluene.[20] The high surface to volume ratio makes the entire nanocrystal lattice accessible to solid-state diffusion. Thus, the transformation occurs spontaneously (<1 sec) at room temperature, and is apparent by a color change (from red to brown) due to different bandgap energies of CdSe and Ag_2Se. Furthermore, the exchange reaction can be reversed to obtain the original bright red solution of CdSe nanocrystals, leading to the near complete recovery of the original exciton spectrum, with only a small change in size-dependent features. By manipulating the ion solubility with coordinating molecules, here we show that the reverse reaction (conversion from the 1+ to 2+ cation) can provide a pathway to new materials.

The thermodynamic driving force for exchange between two cations can be controlled by the solvent and surfactant system based on their relative solvation energies with a particular coordinating species.[20,21] In the CdSe – Ag_2Se pair, the forward exchange (from CdSe to Ag_2Se), is thermodynamically driven by the preferential solvation of Cd^{2+} ions relative to Ag^+ in methanol (MeOH). The reverse exchange from Ag_2Se to CdSe is favored by the addition of Cd^{2+}, along with tributylphosphine (TBP). These exchange reactions can be qualitatively understood in terms of Hard Soft Acid Base theory, where the monovalent Ag^+ cation is softer than the divalent Cd^{2+} cation.[22] Thus, MeOH, a hard base, preferentially binds Cd^{2+} cations, while the soft base, TBP, binds strongly to Ag^+ cations. Several other examples of Cd^{2+} exchange in CdS(Se,Te) nanocrystals with comparatively soft metal ions (Cu^+, Pd^{2+}, Pt^{2+}, Hg^{2+})[18,21,23] using MeOH or water as the solvent and the replacement of soft Ag^+ in Ag_2S nanocrystals with

harder metal ions (Pb^{2+}, Zn^{2+}) using TBP have demonstrated the generality of this method.[24] While we were not able to find conditions to directly convert CdS to PbS (due to the similarity of the two ions in their valency, hardness, and electronegativity),[25] through the intermediate conversion of CdS to Cu_2S or Ag_2S, we manipulate the system to produce PbS which retains the original anisotropic nanocrystal shape.

We employed exchange reactions to sequentially convert CdS nanocrystals first to Cu_2S and then PbS following the reactions schemes:

1) $CdS_{toluene} + 2\ Cu^{+}(MeOH) + 2\ PF_6^{-}(MeOH) \rightarrow Cu_2S_{toluene} + Cd^{2+}(MeOH) + 2\ PF_6^{-}(MeOH)$
2) $Cu_2S_{toluene} + Pb^{2+}(MeOH) + 2\ OAc^{-}(MeOH) + 2\ TBP_{toluene} \rightarrow PbS_{toluene} + 2\ Cu^{+}(TBP) + 2\ OAc^{-}(MeOH)$

where PF_6^{-} is the hexafluorophosphate anion of the copper salt, and OAc^{-} is the acetate anion of the lead salt, subscripts indicate suspension whereas the parenthesis denote solvation. Analogous to the examples of cation exchange reactions described above, the exchange of Cu^{+} with CdS is promoted with MeOH. After isolation of the nanocrystal product, the exchange of Pb^{2+} with Cu_2S nanocrystals is then performed by adding Pb^{2+} and TBP.

During the diffusion and exchange of cations, the anion sublattice is relatively stable, leading to two important consequences. 1) The shapes of anisotropic nanocrystals are generally preserved upon cation exchange, as long as the minimum dimensions of the nanocrystal are greater than the reaction zone of the exchange process.[20] 2) A topotaxial relationship exists between the initial and final materials.[18,20] Thus, if the exchange reaction is limited to only

part of the nanocrystal, a heterostructure is produced where the different compositions share a continuous anion framework.

The synthesis of monodisperse cadmium chalcogenide nanocrystals with controllable lengths and diameters has been extensively studied over the last decade, making it a well-suited template material for ion exchange conversion.[26-29] While some shape control of lead chalcogenide nanocrystals has also been demonstrated, they typically have cubic or octahedral symmetry, owing to their cubic crystal structure.[30] Elongated structures have been synthesized through oriented attachment of PbSe particles into linear chains, but this approach allows for little length control.[31] The full sequential cation exchange process shown here leads to superior monodispersity of the PbS nanorods.

We demonstrate that through the intermediate conversion of CdS to Cu_2S, the fraction of the ends of rod-shaped nanocrystals converted to PbS can also be controlled. Alternatively, partial Ag^+ exchange can serve as the intermediate step, which produces a striped or superlattice heterostructure morphology.[17] Thus, the spatial arrangement of the components of the heterostructure (i.e. end-on conversion of the nanorod versus striped structure) is controlled via the first exchange reaction, and the final composition is determined by the second. Complete sequential cation exchange also allows the optical properties of one nanocrystal material to another with the same size and shape to be compared directly.

We first discuss a control experiment to properly characterize that NC size is preserved in the reverse reactions from Cu_2S to PbS or CdS. We synthesized spherical Cu_2S nanocrystals with the high chalcocite phase following Wu et al.[32] Monodisperse Cu_2S nanocrystals with diameters <5 nm are then suspended in toluene for the cation

exchange reactions. Transmission electron microscopy (TEM) provides the best measure of NC size because of a relative lack of optical absorbance features, a complex X-ray diffraction (XRD) spectrum with no well-resolved peak to measure, and relatively few publications on size/shape control (See Ref. 32 and Refs therein). Following a similar method for Ag_2Se to CdSe exchange described above, Cu_2S nanocrystals are then transformed to PbS or CdS where the size dependent optical properties can be compared.

To convert Cu_2S to PbS or CdS, a solution of Pb^{2+} or Cd^{2+} ions with TBP was prepared, and was then added to Cu_2S NCs in toluene, and allowed to stir for ~2 hours while the color changed from orange-brown to either dark brown for PbS or bright yellow for CdS. The NCs were then separated from the free-floating ions by centrifugation (see Materials and Methods). Figure 1 shows TEMs along with XRD and UV-vis for NCs in all three sulfide compositions (CdS, Cu_2S and PbS). The TEMs show well packed, monodisperse particles with similar diameter, aside from small deviations for differing lattice constants of the 3 crystals. Perhaps a better indication of the NC size is inferred by the linear absorption data correlated to published size-dependent extinction coefficients for the well-studied lead and cadmium chalcogenides. Figure 1d shows the absorbance curves for spherical particles. CdS exhibits several sharp excitonic features indicating the high degree of monodispersity. The first exciton peak occurs at 440 nm (2.81 eV), corresponding to a diameter of 4.85 nm.[33] PbS has small effective masses for electrons and holes which leads to a dramatic blueshift in the bandgap above the bulk value of 0.41 eV when confined below 20 nm and displays a wealth of fascinating properties at the nanoscale.[34-37] In the case of our spherical PbS particles created by cation exchange from Cu_2S, the first exciton peak

occurs at 1240 nm (1 eV) and corresponds to NCs with diameter of 4.8 nm.[38,39] XRD patterns of the three samples show the initial Cu_2S in the high temperature chalcocite phase, while the CdS and PbS nanocrystals are in the wurtzite and rock salt phase, respectively. The particle sizes are also verified by applying a Debye-Sherrer fit to the XRD data in Fig. 1e.[40]

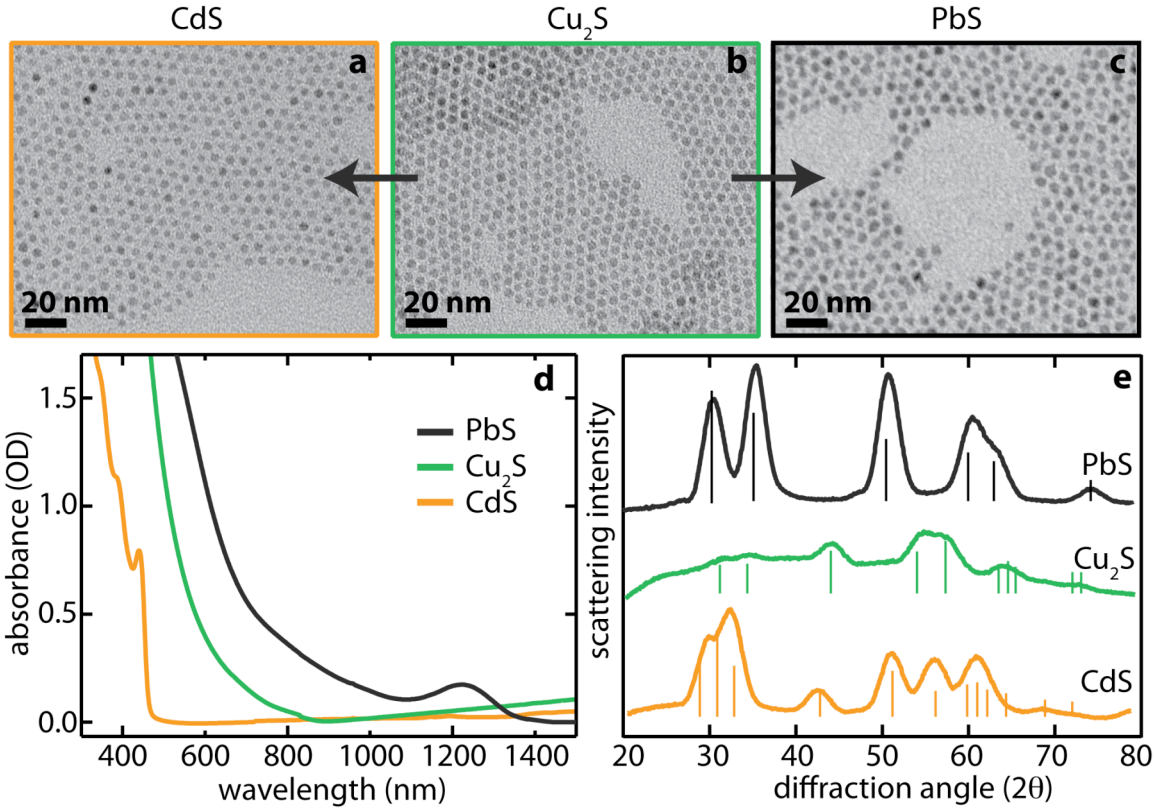

Figure 1|Properties of Cu_2S spherical particles converted to CdS and PbS. a-c, TEM images of well packed CdS, Cu_2S, and PbS nanocrystals, respectively. Images are at the same magnification with a scale bar of 20 nm in each image. **d**, Identical concentration absorption spectra for nanocrystals of CdS, Cu_2S and PbS from the same starting material in tetrachloroethylene. The characteristic first exciton peak for CdS (PbS) is at 440 nm (1240 nm) corresponding to a nanocrystal diameter of ~4.8 nm. **e**, XRD for an ensemble of nanocrystals of Cu_2S (green). Also shown are the CdS (orange) and PbS (black) resulting from cation exchange of Cu_2S. The JCPDS card file for each material is shown below the spectrum for identification.

After verifying that Cu_2S can readily be converted to PbS, we then synthesized highly anisotropic rod-shaped CdS nanocrystals by

using multiple surfactants.[28] Recently we have shown that Cu^{+} ions will readily exchange with Cd^{2+} by selectively targeting the nanorods' more reactive end facets. We exchanged CdS nanorods to Cu_2S nanorods using this same procedure.[18] The resulting Cu_2S nanocrystals are isolated and then exchanged to PbS just as described above for spherical Cu_2S to PbS conversion. Figure 2a-c shows TEMs of the nanorods throughout the sequential cation exchange. The absorbance spectra for solutions of the nanorods are shown in Fig. 2d. The exciton features in the CdS spectrum result from the highly monodisperse nanorod diameter throughout the sample. Since the diameter is much smaller than the length, quantum confinement effects are dominated by this dimension.[5,27] Upon conversion to Cu_2S, a weak exciton peak arises at 850 nm. After the sequential cation exchange to PbS, a well-resolved peak at 1440 nm appears. While, several reports exist for rod-shaped PbS crystals,[41-45] no reports to date show featured quantum confined absorption spectra in any of the lead chalcogenides for such anisotropic shapes. This is presumably due to the difficulty of growing highly symmetric rock salt crystals into monodisperse nanorods. Here we take advantage of the abundance of preexisting work on shape control in cadmium chalcogenides to control the final size and shape of lead chalcogenide crystals with sequential chemical transformations.

The first exciton peak at 1440 nm (0.86 eV) corresponds to spheres with a diameter of 5.7 nm,[38] yet the nanorods produced have a diameter of <5 nm with average length of ~28 nm. Figure 2e shows the XRD patterns for each of the nanorod samples along with the JCPDS card files to identify each material. The XRD provides the best evidence that the final nanorods are rock salt PbS, and is supported by typical a PbS absorption spectrum shown in Fig. 2d. Furthermore, just

as in the case for cadmium chalcogenides, the bandgap can be tuned by varying the diameter of the nanorod.[27] In Supplementary Information (Fig. S1) additional absorption spectra shows that the bandgap can be increased greater than 1 eV (i.e. increased confinement) with decreasing diameter, independent of the length.

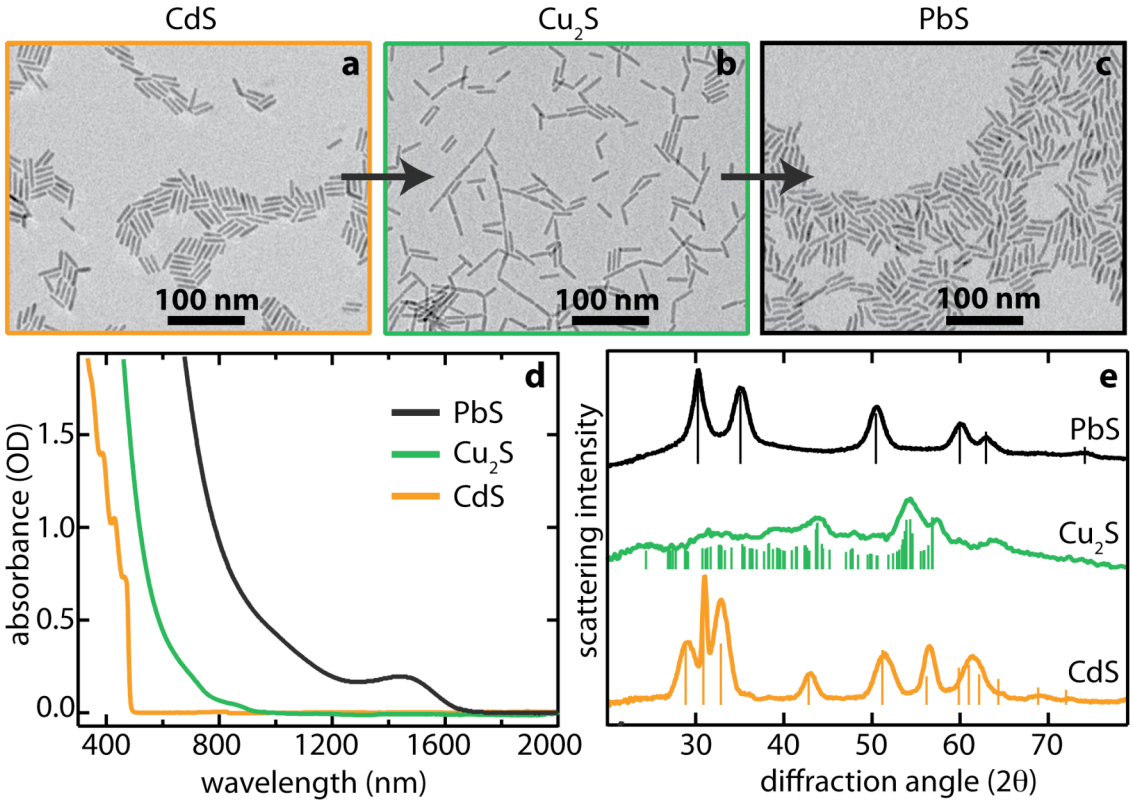

Figure 2|Properties of nanorods of CdS transformed into Cu_2S and then PbS. TEM images of as-synthesized CdS **a**, intermediate Cu_2S **b**, and final PbS **c,** nanorods. The scale bars are 100 nm long and the arrows indicate the order of cation exchange products. **d**, Absorption spectra for CdS (orange), Cu_2S (green), and PbS (black) nanorods with identical concentration. **e**, XRD patterns for the different materials. The lines under the spectra are the JCPDS patterns for each material. Here, we assign the Cu_2S nanorods to the low chalcocite phase.[18]

The degree of cation exchange in nanorods from CdS to Cu_2S can be controlled by the amount of Cu^+ ions added to the solution.[18] For example, if the ratio of Cu^+:Cd^{2+} is restricted to 1, then, on average, the nanorods are composed of 50% CdS and 50% Cu_2S

(because two Cu^+ cations are needed to replace each Cd^{2+} cation for charge balance). Here, we followed this procedure to create a series of heterostructured nanorods from the same CdS sample as in Fig. 2a to have varying amounts of Cu_2S within each nanorod. Each was then exposed to an excess of Pb^{2+} ions (the same amount as used for the full exchange in Fig. 2). We find that the final nanoheterostructures are composed only of CdS and PbS, where only the Cu_2S segments have been converted to PbS. Figure 3 shows basic characterization of CdS|PbS nanorod heterostructures as a function of the amount of Cu^+ ions that were added to the CdS solution. While previous work has shown the conversion of lead chalcogenides directly to cadmium chalcogenides (the reverse transformation of our work, limited to spheres), these reactions were explained by stronger bonding of the Cd-chalcogenide lattice, rather than the relative solubility of the ions.[46,47] Our experiment demonstrates that the reaction of CdS + Pb^{2+} $\rightarrow$ PbS + Cd^{2+} is far less favorable under our conditions than Cu_2S + Pb^{2+} $\rightarrow$ PbS + $2Cu^+$ (see reaction scheme above). Presumably, the soft base, TBP, binds more strongly to the monovalent Cu^+ cation compared to Cd^{2+} or Pb^{2+} providing substantially more control.

In Fig. 3a, the XRD patterns of nanocrystals only show contributions from CdS and PbS and are clearly a convolution of the two diffraction patterns, where the relative fraction of each is controlled by the amount of Cu^+ ions added in the intermediate step and is independent of the amount of Pb^{2+} ions added. Upon exposing CdS to an increasing Cu^+:Cd^{2+} ion ratio, the CdS to Cu_2S conversion proceeds further, and the resulting nanocrystals show diffraction patterns with more PbS than CdS indicated by the decrease in the peaks at 2θ = 43° and 57° and the appearance of 2 distinct peaks instead of 3 near 2θ = 30°.

A much different morphology of CdS|PbS nanorods is created by using Ag^+ ions as the intermediate, rather than Cu^+. In this case the partial exchange into CdS|Ag_2S leads to Ag_2S segments distributed along the CdS nanorod walls and under careful conditions leads to a superlattice structure in each nanorod with alternating segments of CdS and Ag_2S.[17,48] Thus, the intermediate stage can be used to control the resulting heterostructured topology as only the Ag^+ ions are replaced by Pb^{2+} leading to PbS embedded in CdS, see Supplementary Information Fig. S2.

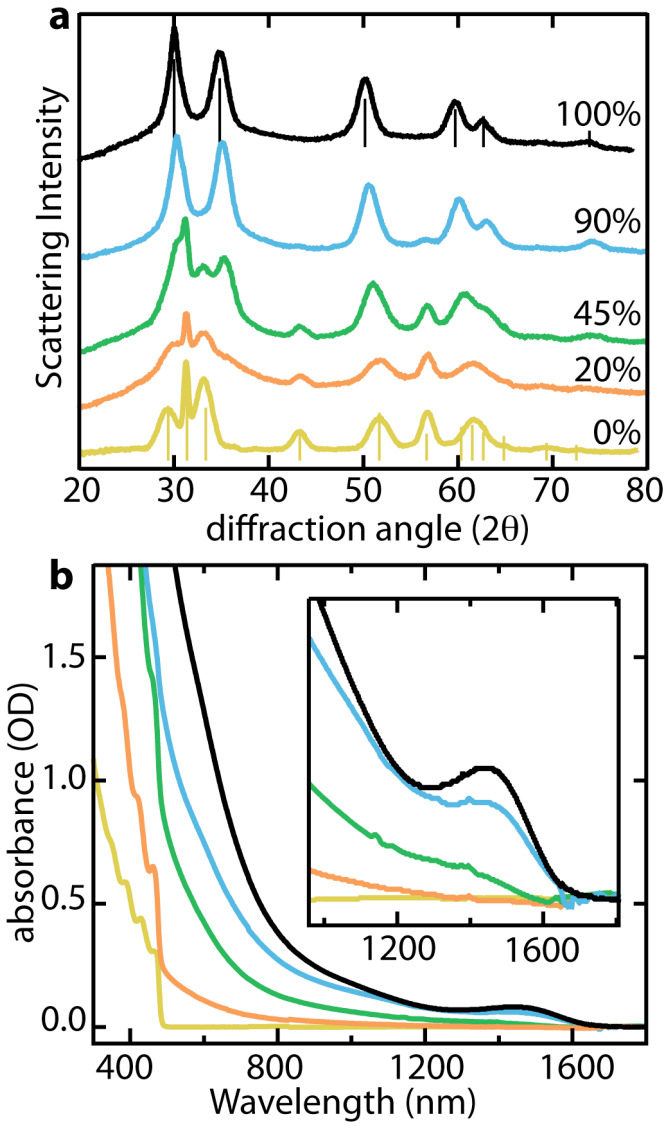

Figure 3|Heterostructured nanorods of CdS|PbS. a, XRD spectra for nanorods of CdS that have been partially converted to Cu_2S before being exposed to Pb^{2+} ions. The nanorods are a mixture of wurtzite CdS and rock salt PbS. The JCPDS card files for CdS (yellow) and PbS (black) are shown under the according spectra. **b**, Absorption spectra of heterostructured CdS|PbS nanorods. Nanorods partially exchanged to Cu_2S and then to PbS show absorbance features, which resemble a superposition of that for PbS and CdS. However, the intensity and peak position of the PbS first exciton peak is dependent on the amount of Cu^+ ions added during the intermediate step.

The absorption spectrum of the heterostructured nanorods is shown in Fig. 3b. For low conversion ratios, the absorption closely resembles CdS with a characteristic cutoff to the red of 470 nm and a tail extending red, due to the smaller bandgap of PbS. Upon further conversion, the absorbance onset redshifts and develops a well-structured exciton peak at 1440 nm.

Due to the differing crystal structures of wurtzite CdS (hexagonal lattice with 4 nearest neighbor atoms) and rock salt PbS (cubic lattice with 6 nearest neighbor atoms), we employed high resolution TEM (HRTEM) to examine the structure of nanorods fully converted from CdS to PbS (Fig. 4) and partially converted nanorods to study the interface between the two crystal structures (Fig. 5).

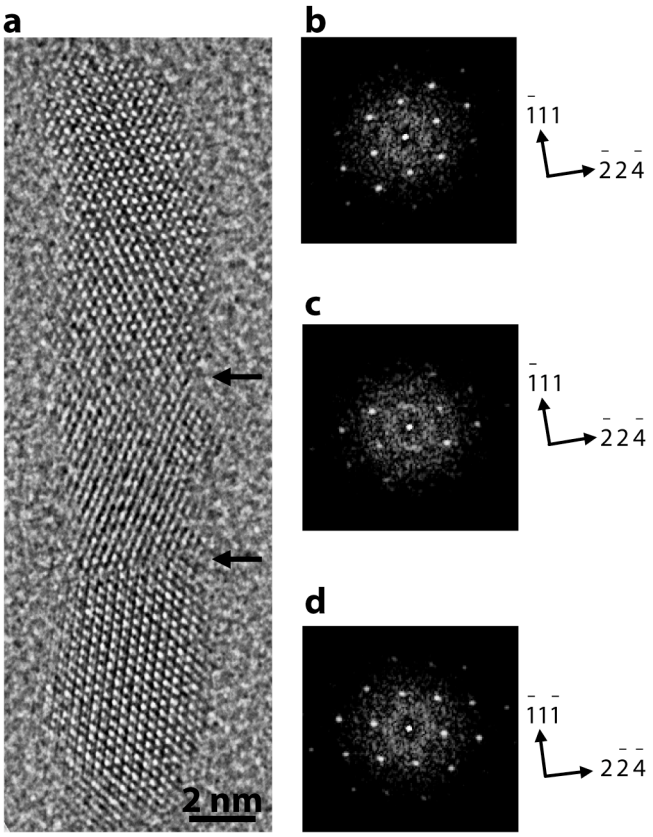

Figure 4|Fully converted PbS nanorod. a, HRTEM image of a fully converted PbS nanorod. Arrows indicate grain boundaries. **b-d**, FFT patterns of the top, middle, and bottom sections of the nanorod as separated by the arrows in a). Each FFT pattern shows a well-defined diffraction pattern corresponding to the [110] zone diffraction of a rock salt PbS crystal.

Figure 4 shows a high resolution TEM image of a 25 × 4.5 nm PbS nanorod. We observe grain boundaries appearing in the fully exchanged PbS nanorods. However fast Fourier transform (FFT) of the single grains (as shown in Fig. 4b-d) show that all regions are PbS of the same rock salt phase with an in-plane rotation between the grains. We note that since the S sublattice of Cu_2S is very similar to CdS, there is little change in the shape of the nanorods during cation exchange between Cu^+ and Cd^{2+}.[18] By studying the heterostructured CdS|PbS rods from partial exchange of CdS to Cu_2S, we can understand the formation of such "multigrain" morphology of PbS nanorods. Figure 5 shows an HRTEM image of a nanorod having

undergone partial exchange to Cu_2S followed by conversion of the Cu_2S portion to PbS. The Cu_2S is completely removed and the resulting particle has a rock salt PbS grain attached epitaxially to the wurtzite CdS phase, with $(\bar{1}11)_{PbS}//(00\bar{2})_{CdS}$ and $(\bar{2}2\bar{4})_{PbS}//(1\bar{1}0)_{CdS}$. Epitaxial connections between wurtzite and rock salt phases of nanocrystals have been seen and discussed in literature.[14,46,47,49] The atomic structure and interface that are built based on such observations (Fig. 5f) show lattice distortions of the S frame in addition to the displacement of cations between the two phases. As the exchange front moves along the nanocrystals during the reaction, such displacement induces the misalignment of the long axis of PbS relative to that of CdS, see Fig. 5a. Cation exchange may start from both ends of the nanorods with different lattice distortions, as shown in case of CdS to Cu_2S.[18] Therefore as the reaction fronts meet, a grain boundary can form. As seen in the fully converted PbS nanorod in Fig. 4 the FFT of part b and c are the same face and orientation and part c shows a different orientation. The grains meet at the lower of the 2 arrows in part a. In the case of heterostructured particles, the PbS segments are a single crystalline (Fig. 5a).

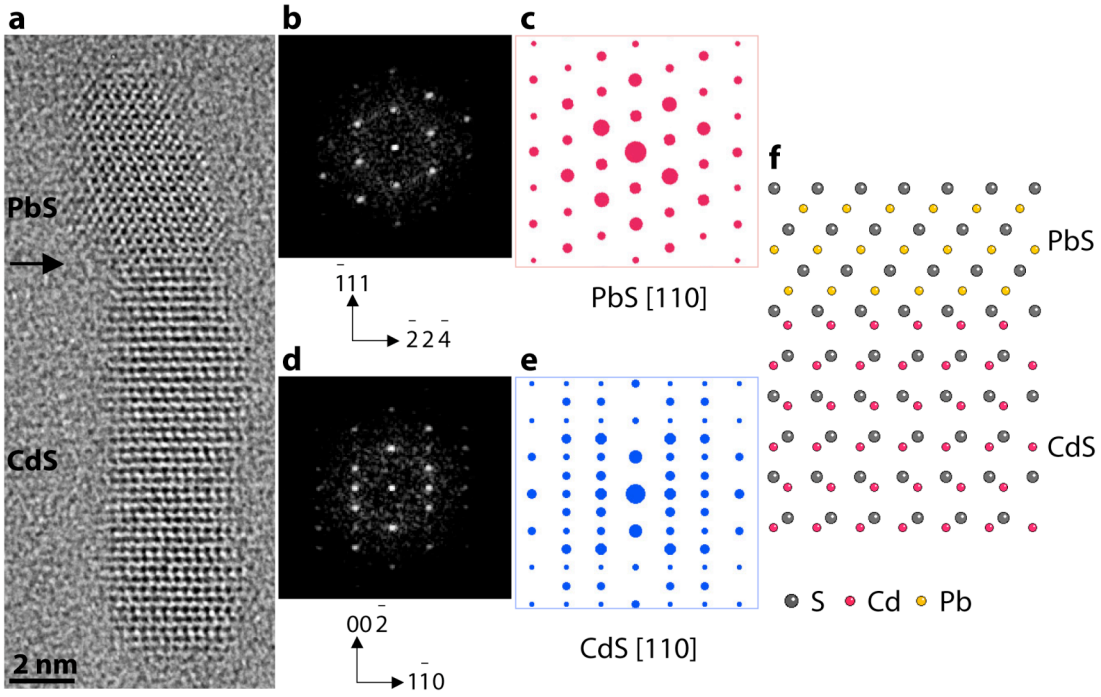

Figure 5|High-resolution TEM image and simulated atomic structure displaying the interface of CdS|PbS nanoheterostructures. a, High resolution TEM image showing epitaxy between rock salt PbS and wurtzite CdS. An arrow highlights the interface. **b**, FFT pattern of the PbS grain in a). **c**, The simulated diffraction pattern of rock salt PbS [110]. **d**, FFT pattern of the CdS grain in a). **e**, The simulated diffraction pattern of wurtzite CdS [110]. **f**, Atomic structure and interfacial model between PbS and CdS viewed from [110] of both phases.

The long dimension of the CdS nanorods is the [002] direction as can be verified by the FFT shown in Fig. 5c. Correspondingly, the sharpest peak in the XRD pattern at $2\theta = 32°$ belongs to the (002) plane in Fig. 3a (bottom trace). Upon cation exchange to PbS, we use FFT images of the high-resolution TEM images to confirm that the elongated dimension of CdS transforms to the [111] direction of PbS. The XRD for the completely exchanged PbS rods in Fig. 3a shows a sharpened (111) peak at $2\theta = 29°$, due to longer diffraction coherence.

We have shown the ability to independently control the shape, topology and final chemical composition of colloidal nanocrystals in

three separate steps. The nucleation and growth of the nanocrystal starting material determines the shape, while a sacrificial exchange into an intermediary composition allows for conversion to a heterostructure containing two materials with control of their topology. The second exchange reaction determines the final chemical composition of the crystal. This method has enabled the construction of the first example of highly monodisperse PbS nanorods that will undoubtedly be useful materials for various applications. By precisely controlling ion insertion and removal (through partial Cu^+ or Ag^+ exchange) nanorod heterostructures with different morphologies can be obtained. The selectivity for the second exchange reaction to convert only the Cu_2S (Ag_2S) portion of the heterostructures to PbS is akin to regioselective transformations of functional groups in organic molecules. Such selectivity is essential for the creation of complicated nanostructures over multistep synthesis. The successive cation exchange principle demonstrated here provides a unique route to synthesize epitaxial heterogeneous nanostructures in a variety of material combinations and shapes.

Materials and Methods.

Spherical Cu_2S nanoparticles are prepared by a slightly modified version of Wu et al.[32] 104 mg of ammonium diethyldithiocarbamate (Aldrich), 10 ml 1-dodecanethiol (≥98% (Aldrich)), 14 ml oleic acid (technical grade, 90% (Aldrich)) are combined in a 50 ml flask and heated to 180° C under argon flow. In a separate flask 610 mg of copper (II) acetylacetonate (≥99.99% trace metals basis (Aldrich)) and 7 ml of oleic acid are heated under argon to 110° C. As soon as the solutions are homogeneous and temperatures are stable, 6 ml of the Cu solution are removed *via* syringe and injected into the other flask. The solution is allowed to react at 180° C for 6 min and then the heat is removed. Upon cooling, the black solution is transferred air-free into a vial and centrifuged at 4000 rpm for 5 min. The supernatant is discarded and the precipitated product is redispersed in hexane and extracted by adding methanol and

centrifuging. The final product after several three cleaning cycles is roughly 75 mg and suspended in 10 ml of toluene. For reference, the absorbance of the concentration used in the reaction is shown in Supplementary Information Fig. S3a.

Cu_2S Spheres are converted to PbS and CdS by room temperature addition of new cations similar to the reverse exchange by Son et al.[20] to convert Ag_2Se back to CdSe. An ion exchange stock solution is prepared to make the conversion more straightforward. First, a 0.15 mM solution of cations is prepared by addition of lead (II) acetate trihydrate (99.999% trace metals basis (Aldrich)) for PbS or cadmium nitrate tetrahydrate (purum p.a., ≥99.0% (Fisher)) for CdS in methanol. Once dissolved, an equal amount of 0.26 mM solution of tri-n-butylphosphine (99% Strem, TBP) in toluene is added. TBP is used to promote the exchange in Cu_2S nanocrystals, by binding strongly to Cu^+ ions, thus creating a driving force to convert the crystal into PbS or CdS. Control experiments without the use of TBP show extremely slow kinetics or no ion exchange. To perform the exchange, 1 ml of toluene is added to 0.1 ml of the stock solution of Cu_2S nanocrystals in a vial on a stirring plate (with magnetic stir bar) in a glovebox. 1 ml of the ion exchange solution is added. To aid in the solubility of the final product, we also add 10-30 μl of lead oleate or cadmium oleate. These solutions are prepared by following Pietryga[47] and are stored in a vial in the glovebox on a hotplate at 80° C. 2 ml of methanol is added before centrifuging at 3000 rpm to separate the nanocrystals from the solvent and ions. The final product is soluble in nonpolar organic solvents.

CdS nanorods are made following Robinson and Sadtler.[17,18] In brief, 210 mg CdO (≥99.99% trace metals basis (Aldrich)), 2.75 g tri-n-octylphosphine oxide (99% (Acros)), 1.06 g n-octadecylphosphonic acid (PolyCarbon Industries) are heated in a 25 ml flask to 120° C under vacuum for 30 min. Argon is introduced and the solution is heated to 320 for 20 min and cooled again to 125° C and held under vacuum for 30 min. A stock solution of equimolar tri-n-octylphosphine (97% (Strem)) and sulfur (flakes, ≥99.99% trace metals basis (Aldrich)) (TOP|S) is previously prepared and allowed to stir for 1 day in a glovebox. The temperature of Cd-phosphonate is raised to 320° C and 1.5 g of TOP and 1.5 g of TOP|S is added via syringe and allowed to react for 45 min at 315° C. The solution is then cooled to room temperature, 10 ml toluene is added, and placed in a centrifuge at 4000 rpm for 10 min. The supernatant is separated and the product is redispersed in 5-7 ml of toluene and 2

ml of nonanoic acid (purum, ≥97.0% (GC) (Fluka)). Hexane is added (~15 ml) slowly until the solution is clear and then 15 ml of methanol is added and the solution is centrifuged at 4000 rpm for 10 min. The last step is repeated twice and a stock solution of the CdS rods is made by dispersing the resulting product in toluene. For reference, the absorbance of the concentration used in the cation exchange reaction is shown in Supplementary Information Fig. S3b.

Partial and full exchange of CdS nanorods to Cu_2S is well described by a previous report by Sadtler et al.[18] In this case, a solution of tetrakis (acetonitrile) copper(I) hexafluorophosphate (Aldrich) is made in methanol. 0.5 ml is added to 0.5 ml toluene and under rapid stirring, 100 μl of the CdS stock solution is added. The color instantly changes to orange-brown, the vial is then centrifuged at 3000 rpm and the product is suspended in 1 ml of toluene. The concentration of the methanolic solution determines the fraction of the sample converted to Cu_2S. In this case we found 2 mg/ml to completely convert the rods to Cu_2S by XRD and UV-vis characterization. Partial exchange was performed by varying the amount of Cu^+ in the solution relative to the 2-mg/ml mark. For full exchange 10 mg/ml was used to assure that the entire sample was converted to Cu_2S.

The conversion of the Cu_2S or Ag_2S portions of nanorods to PbS is accomplished similar to the conversion of Cu_2S spheres to PbS**.** The Cu_2S rods in 1 ml of toluene were converted to PbS rods by using the same cation stock solutions as in the case of the spheres. Only 1 ml of methanol is added before centrifugation to separate the nanorods.

Interfacial model. The electron diffraction patterns and interface structure were simulated using commercially available software Crystalkit (http://www.totalresolution.com).

Instrumentation. Absorbance measurements are performed with the nanocrystals suspended in tetrachloroethylene (ACS reagent, ≥99.0% (Sigma-Aldrich)) on a Shimadzu 3600 UV-Vis-NIR spectrophotometer. Low-magnification TEM images were acquired with a 200kV LaB6 FEI Tecnai G2 20 HRTEM, equipped with a Super TWIN lens. FFT algorithms performed using freeware ImageJ software http://rsbweb.nih.gov/ij/index.html. For high resolution, a 200 kV FEI

monochromated F20 UT Tecnai TEM equipped with a field emission gun, a High Angle Annular Dark Field detector (HAADF), and a Gatan Image Filter (GIF) was also used for the TEM characterization. Powder XRD characterization was carried out on a GADDS Hi-Star D8 diffractometer (Bruker) using CoKα radiation (1.790 Å) and a general area detector. Samples were prepared by deposition on a quartz plate with background subtraction. Accumulation time for each sample was 20 min (10 min per frame). Experimental XRD patterns were compared with those published in the Joint Committee of Powder Diffraction Standards PDF database for bulk materials (CdS: no. 41-1049; PbS: no. 05-0592; Cu_2S: nos. 26-1116, 33-0490).

Acknowledgement

This work was funded by the Helios Solar Energy Research Center, which is supported by the Director, Office of Science, Office of Basic Energy Sciences, Materials Sciences and Engineering Division, of the U.S. Department of Energy under Contract No. DE-AC02-05CH11231. The authors acknowledge the National Center for Electron Microscopy for providing the advanced electron microscopy facilities for this work.

References

1. Jun, Y.W., Choi, J.S. & Cheon, J. Shape control of semiconductor and metal oxide nanocrystals through nonhydrolytic colloidal routes. *Angewandte Chemie-International Edition* **45**, 3414-3439 (2006).

2. Burda, C., Chen, X., Narayanan, R. & El-Sayed, M.A. Chemistry and Properties of Nanocrystals of Different Shapes. *Chemical Reviews* **105**, 1025-1102 (2005).
3. Alivisatos, A.P. Semiconductor clusters, nanocrystals, and quantum dots. *Science* **271**, 933-937 (1996).
4. Kanaras, A.G., Sonnichsen, C., Liu, H.T. & Alivisatos, A.P. Controlled synthesis of hyperbranched inorganic nanocrystals with rich three-dimensional structures. *Nano Letters* **5**, 2164-2167 (2005).
5. Manna, L., Milliron, D.J., Meisel, A., Scher, E.C. & Alivisatos, A.P. Controlled growth of tetrapod-branched inorganic nanocrystals. *Nature Materials* **2**, 382-385 (2003).
6. Huynh, W.U., Dittmer, J.J. & Alivisatos, A.P. Hybrid nanorod-polymer solar cells. *Science* **295**, 2425-2427 (2002).
7. Hu, J.T.*, et al.* Linearly polarized emission from colloidal semiconductor quantum rods. *Science* **292**, 2060-2063 (2001).
8. Jin, R.C.*, et al.* Photoinduced conversion of silver nanospheres to nanoprisms. *Science* **294**, 1901-1903 (2001).
9. Link, S. & El-Sayed, M.A. Spectral properties and relaxation dynamics of surface plasmon electronic oscillations in gold and silver nanodots and nanorods. *Journal of Physical Chemistry B* **103**, 8410-8426 (1999).
10. Cui, Y., Banin, U., Bjork, M.T. & Alivisatos, A.P. Electrical transport through a single nanoscale semiconductor branch point. *Nano Letters* **5**, 1519-1523 (2005).
11. Tian, B.Z.*, et al.* Coaxial silicon nanowires as solar cells and nanoelectronic power sources. *Nature* **449**, 885-U888 (2007).
12. Trudeau, P.E., Sheldon, M., Altoe, V. & Alivisatos, A.P. Electrical contacts to individual colloidal semiconductor nanorods. *Nano Letters* **8**, 1936-1939 (2008).
13. He, J., Lo, S.S., Kim, J.H. & Scholes, G.D. Control of Exciton Spin Relaxation by Electron-Hole Decoupling in Type-II Nanocrystal Heterostructures. *Nano Letters* **8**, 4007-4013 (2008).
14. Kudera, S.*, et al.* Selective growth of PbSe on one or both tips of colloidal semiconductor nanorods. *Nano Letters* **5**, 445-449 (2005).
15. Mokari, T., Sztrum, C.G., Salant, A., Rabani, E. & Banin, U. Formation of asymmetric one-sided metal-tipped semiconductor nanocrystal dots and rods. *Nature Materials* **4**, 855-863 (2005).
16. Smith, A.M., Mohs, A.M. & Nie, S. Tuning the optical and electronic properties of colloidal nanocrystals by lattice strain. *Nature Nanotechnology* **4**, 56-63 (2009).
17. Robinson, R.D.*, et al.* Spontaneous superlattice formation in nanorods through partial cation exchange. *Science* **317**, 355-358 (2007).
18. Sadtler, B.*, et al.* Selective Facet Reactivity during Cation Exchange in Cadmium Sulfide Nanorods. *Journal of the American Chemical Society* **131**, 5285-5293 (2009).
19. Dloczik, L. & Konenkamp, R. Nanostructure transfer in semiconductors by ion exchange. *Nano Letters* **3**, 651-653 (2003).
20. Son, D.H., Hughes, S.M., Yin, Y.D. & Alivisatos, A.P. Cation exchange reactions-in ionic nanocrystals. *Science* **306**, 1009-1012 (2004).
21. Wark, S.E., Hsia, C.H. & Son, D.H. Effects of ion solvation and volume change of reaction on the equilibrium and morphology in cation-exchange reaction of nanocrystals. *Journal of the American Chemical Society* **130**, 9550-9555 (2008).

22. Martell, A.E.H., Robert D. *Metal Complexes in Aqueous Solutions*, (Plenium Press, New York, 1996).
23. Mews, A., Eychmuller, A., Giersig, M., Schooss, D. & Weller, H. Preparation, Characterization, and Photophysics of the Quantum-Dot Quantum-Well System CdS/HgS/CdS. *Journal of Physical Chemistry* **98**, 934-941 (1994).
24. Camargo, P.H.C., Lee, Y.H., Jeong, U., Zou, Z.Q. & Xia, Y.N. Cation exchange: A simple and versatile route to inorganic colloidal spheres with the same size but different compositions and properties. *Langmuir* **23**, 2985-2992 (2007).
25. Pearson, R.G. Absolute Electronegativity and Hardness - Application to Inorganic-Chemistry. *Inorg. Chem.* **27**, 734-740 (1988).
26. Jun, Y.W., Lee, S.M., Kang, N.J. & Cheon, J. Controlled synthesis of multi-armed CdS nanorod architectures using monosurfactant system. *Journal of the American Chemical Society* **123**, 5150-5151 (2001).
27. Li, L.S., Hu, J.T., Yang, W.D. & Alivisatos, A.P. Band gap variation of size- and shape-controlled colloidal CdSe quantum rods. *Nano Letters* **1**, 349-351 (2001).
28. Manna, L., Scher, E.C. & Alivisatos, A.P. Synthesis of soluble and processable rod-, arrow-, teardrop-, and tetrapod-shaped CdSe nanocrystals. *Journal of the American Chemical Society* **122**, 12700-12706 (2000).
29. Peng, X.G.*, et al.* Shape control of CdSe nanocrystals. *Nature* **404**, 59-61 (2000).
30. Lee, S.M., Jun, Y.W., Cho, S.N. & Cheon, J. Single-crystalline star-shaped nanocrystals and their evolution: Programming the geometry of nano-building blocks. *Journal of the American Chemical Society* **124**, 11244-11245 (2002).
31. Cho, K.S., Talapin, D.V., Gaschler, W. & Murray, C.B. Designing PbSe nanowires and nanorings through oriented attachment of nanoparticles. *Journal of the American Chemical Society* **127**, 7140-7147 (2005).
32. Wu, Y., Wadia, C., Ma, W.L., Sadtler, B. & Alivisatos, A.P. Synthesis and photovoltaic application of copper(I) sulfide nanocrystals. *Nano Letters* **8**, 2551-2555 (2008).
33. Yu, W.W., Qu, L.H., Guo, W.Z. & Peng, X.G. Experimental determination of the extinction coefficient of CdTe, CdSe, and CdS nanocrystals. *Chemistry of Materials* **15**, 2854-2860 (2003).
34. Ellingson, R.J.*, et al.* Highly efficient multiple exciton generation in colloidal PbSe and PbS quantum dots. *Nano Letters* **5**, 865-871 (2005).
35. Ma, W., Luther, J.M., Zheng, H.M., Wu, Y. & Alivisatos, A.P. Photovoltaic Devices Employing Ternary PbSxSe1-x Nanocrystals. *Nano Letters* **9**, 1699-1703 (2009).
36. McDonald, S.A.*, et al.* Solution-processed PbS quantum dot infrared photodetectors and photovoltaics. *Nature Materials* **4**, 138-142 (2005).
37. Wise, F.W. Lead salt quantum dots: The limit of strong quantum confinement. *Accounts of Chemical Research* **33**, 773-780 (2000).
38. Cademartiri, L.*, et al.* Size-dependent extinction coefficients of PbS quantum dots. *Journal of the American Chemical Society* **128**, 10337-10346 (2006).
39. Hyun, B.R.*, et al.* Electron Injection from Colloidal PbS Quantum Dots into Titanium Dioxide Nanoparticles. *ACS Nano* **2**, 2206-2212 (2008).
40. The TEM images of Fig. 1a-1c are somewhat deceiving because the different cations create stronger contrast for Pb compared to Cd thus making the PbS NCs appear larger than Cu2S or CdS.
41. Chen, M., Xie, Y., Yao, Z.Y., Qian, Y.T. & Zhou, G.E. A novel solvent-directed shape control technique for preparation of rod-shaped PbS crystals. *Materials Research Bulletin* **37**, 247-253 (2002).

42. Li, C.*, et al.* Nonlinear optical properties of the PbS nanorods synthesized via surfactant-assisted hydrolysis. *Materials Letters* **61**, 1809-1811 (2007).
43. Ni, Y.H.*, et al.* Shape controllable preparation of PbS crystals by a simple aqueous phase route. *Crystal Growth & Design* **4**, 759-764 (2004).
44. Wang, S.H. & Yang, S.H. Preparation and characterization of oriented PbS crystalline nanorods in polymer films. *Langmuir* **16**, 389-397 (2000).
45. Warner, J.H. & Cao, H.Q. Shape control of PbS nanocrystals using multiple surfactants. *Nanotechnology* **19**(2008).
46. Lambert, K., De Geyter, B., Moreels, I. & Hens, Z. PbTelCdTe CorelShell Particles by Cation Exchange, a HR-TEM study. *Chemistry of Materials* **21**, 778-780 (2009).
47. Pietryga, J.M.*, et al.* Utilizing the lability of lead selenide to produce heterostructured nanocrystals with bright, stable infrared emission. *Journal of the American Chemical Society* **130**, 4879-4885 (2008).
48. Demchenko, D.O.*, et al.* Formation Mechanism and Properties of CdS-Ag2S Nanorod Superlattices. *ACS Nano* **2**, 627-636 (2008).
49. Zhou, H.S., Honma, I., Komiyama, H. & Haus, J.W. Coated Semiconductor Nanoparticles - The CdS/PbS Systems Synthesis and Properties. *Journal of Physical Chemistry* **97**, 895-901 (1993).

Supplementary Information

for

Independent control of the shape and composition of ionic nanocrystals through sequential cation exchange reactions

Joseph M. Luther, Haimei Zheng, Bryce Sadtler, A. Paul Alivisatos

Materials Science Division, Lawrence Berkeley National Laboratory and Department of Chemistry, University of California, Berkeley

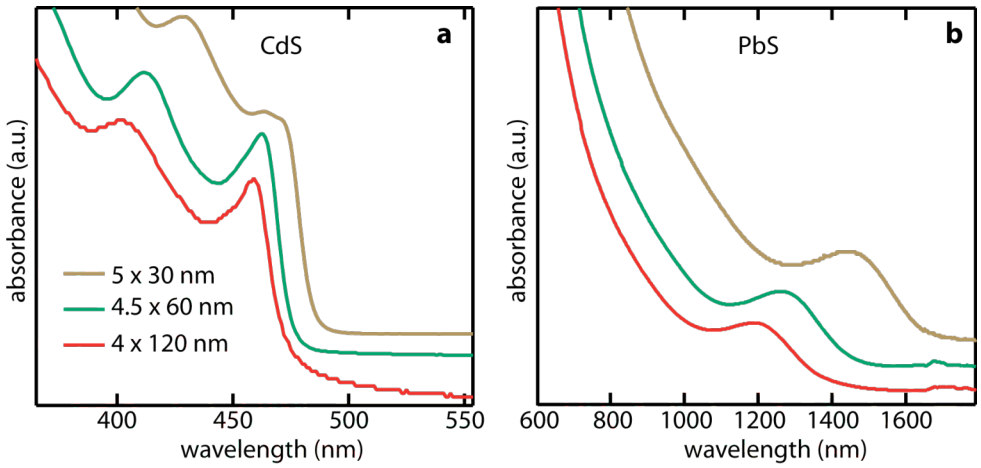

Figure S1|Various starting CdS and converted PbS samples. Absorption spectrum of various sized nanorods of CdS **a,** and the same rods fully exchanged to PbS **b**. The caption lists the average diameter and length of the nanorod, respectively. These spectra demonstrate the tunability of the bandgap of the final PbS by size control of the as-synthesized CdS. The bandgap (or first exciton peak) is mainly governed by the 2 highly confined dimensions.

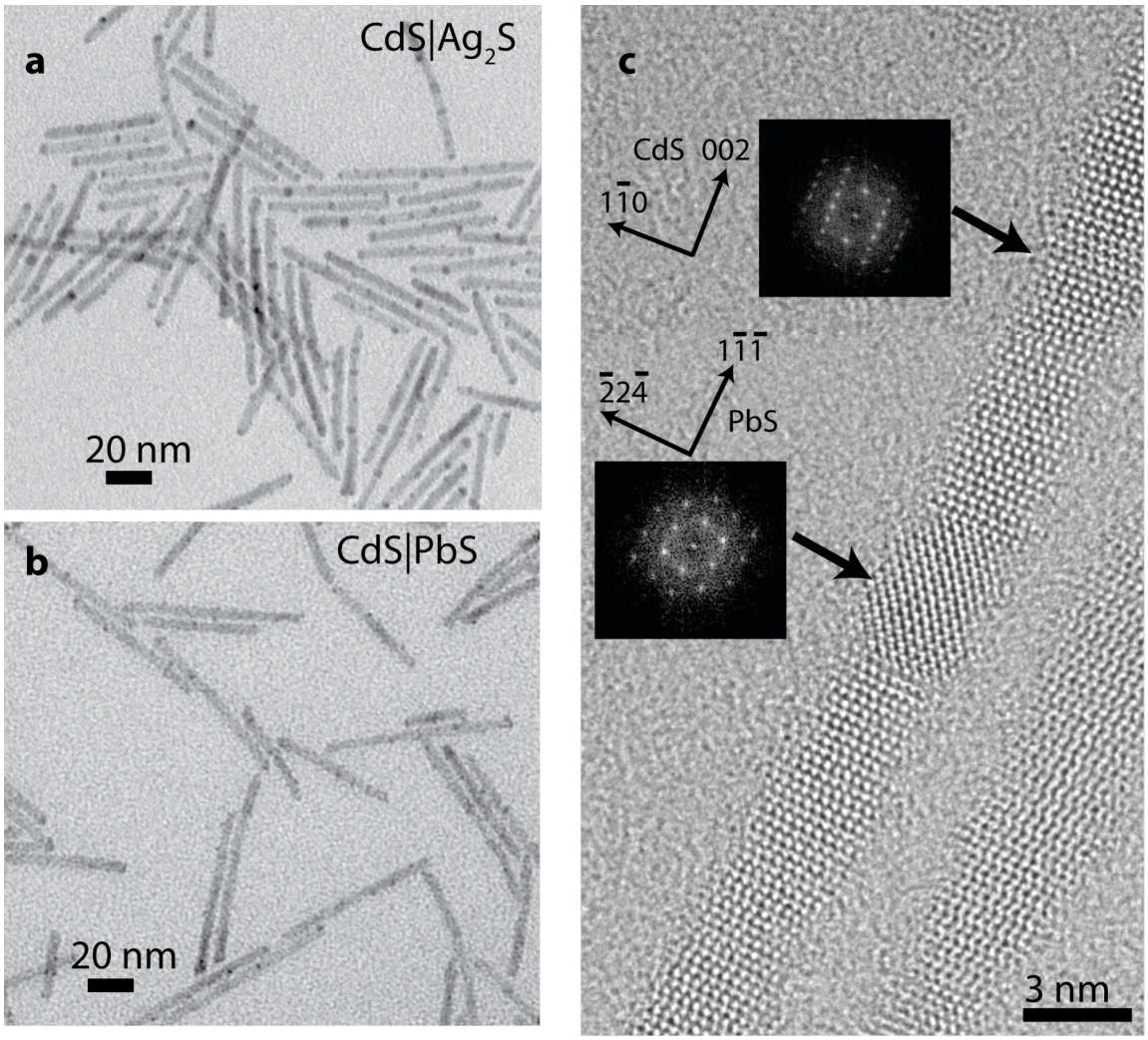

Figure S2|Superlattice structures of CdS|Ag_2S and CdS|PbS. a, TEM image of partial cation exchange into CdS|Ag_2S nanorod superlattice structures following Robinson.[17] Sequentially adding Pb^{2+} ions in the same way as described for the case of CdS|Cu_2S selectively replaces only the Ag^+ ions with Pb^{2+} creating PbS dots embedded periodically throughout the CdS nanorod. This topology is different from the CdS|PbS heterostructures created using Cu^+ as the intermediate ion in that the PbS regions are not only at the ends of the nanorod as in Fig. 5. **b**, TEM image of the final CdS|PbS superlattice structures. The contrast between Pb and Cd containing regions is less obvious than the contrast between Ag and Cd. However high resolution and FFT of various segments of the nanorod clearly demonstrate that PbS sections exist throughout the CdS nanorods as shown in **c**. The lower FFT image shows a rock salt structure different from that of the upper Wurtzite FFT image as well as different from monoclinic Ag_2S. FFT patterns coincide with those shown in Fig. 5b-5e.

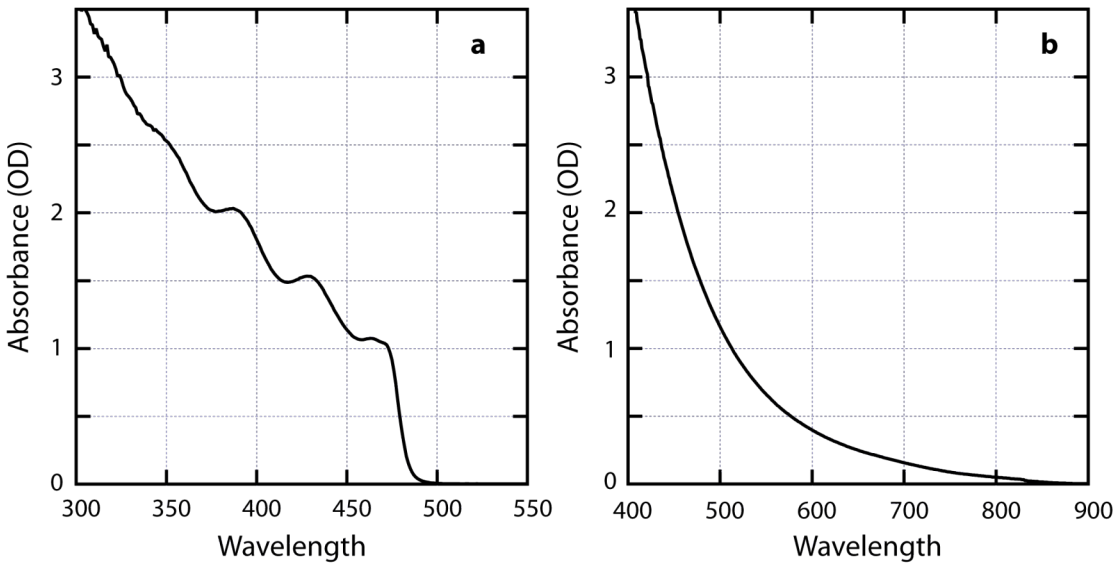

Figure S3|Absorption spectrum of starting materials for cation exchange. a, Absorption spectrum of 0.1 ml of the stock solution of CdS nanorods in toluene plus 1 ml toluene taken through a 2 mm pathlength cuvette. **b**, Absorption spectrum for Cu_2S spherical nanocrystals through a 2 mm pathlength cuvette.